Contribution of lattice parameter and vacancies on anisotropic optical properties of tin sulphide

C.I. Zandalazini [a], J. Navarro Sanchez [a], E.A. Albanesi [a, b], Yashika Gupta [c, d], P. Arun [d, *]

[a] *Instituto de Física del Litoral (IFIS Litoral-CONICET-UNL), Güemes 3450, 3000, Santa Fe, Argentina*
[b] *Facultad de Ingeniería, Universidad Nacional de Entre Ríos, 3101, Oro Verde, Entre Ríos, Argentina*
[c] *Department of Electronics Science, University of Delhi-South Campus, New Delhi, 110 021, India*
[d] *Material Science Research Lab, S.G.T.B. Khalsa College, University of Delhi, Delhi, 110 007, India*

ABSTRACT

Theoretical investigations were made into the band gap, band structure and optical properties of tin sulphide (SnS) crystal with C2mb symmetry. The SnS crystal with this symmetry though has many properties similar to the well documented SnS crystal with *Pnma* symmetry, it does exhibit some uniqueness in band structure. The purpose of this study was to verify and confirm the recent experimental results of p-SnS thin films with C2mb symmetry. The p-type conductivity in SnS films is obtained due to Tin vacancies. These defects invariably gives rise to residual stress in the crystal. Theoretical investigations allow to address the question as to which of the two factors, stress or vacancies with stress, influences the electrical and optical properties more. Results of our calculations confirm that reported p-SnS films were oriented such that the incident light of UV−visible spectroscope fell perpendicular to the 'ab' plane and that shallow levels appear just above the valence band edge along with a spread in the conduction band edge on introduction of defects in the lattice. The spread in conduction band edge and appearance of shallow levels manifest themselves as Urbach spread or tail in UV−visible absorption spectra, which results in a decrease in band-gap with increasing number of Tin vacancies. Calculations also show that while optical properties are essentially due to the Tin vacancies, the residual stress also affects the p-SnS optical properties. The theoretical results are in good agreement with the experimental results.

© 2018 Elsevier B.V. All rights reserved.

1. Introduction

In recent years, tin sulphide (SnS) has been gaining importance due to its potential as a solar cell photo-absorption layer [1,2]. This is due to the high absorption coefficient that it exhibits in its thin film state [3]. The fact that this IV−VI group material is abundantly found and is not toxic are additional attractions [1,4,5]. A lot of work has been done, reporting the characterization of SnS films fabricated by different methods, for example by thermal evaporation [6,7], RF sputtering [8,9], chemical vapor deposition [10,11], electrodeposition [4,12] and spray pyrolysis [13,14] etc. Based on these studies, we now know that SnS in crystalline state is a layered chalcogenide compound with strong anisotropic behavior [1,15,16], whose properties such as band-gap, refractive index etc also depend on the film thickness, grain size, lattice parameters etc [17−19]. For example, the optical band-gap of SnS films lies between 1.1 and 2.1 eV depending on the fabrication method used, which in turn effects grain size, crystal orientation and lattice constants [5,17,20,21].

There are studies which have reported SnS band structure, its band edge positions and thermodynamical stability purely by theoretically considerations using Density Functional Theory (DFT), including Van der Waal's corrections with G_0W_o approximation [22]. Experimental verification of such theoretical results using X-ray Photoelectron spectroscopy (XPS) and inverse photoemission spectroscopy measurements for SnS, SnS_2, Sn_2S_3 have been reported [23]. Other studies based on theoretical considerations have shown that the spin-orbit interactions in SnS produce slight splittings of bands, specially in the conduction band [24]. These studies have also reported the density of states, complex dielectric constants and absorption coefficient of SnS in orthorhombic phase. Green functions and Linear Combinations of Atomic Orbitals (LCAO)

---

* Corresponding author.
  E-mail address: arunp92@sgtbkhalsa.du.ac.in (P. Arun).

have been used to determine the ideal vacancies in SnS, specifically, Sulphur vacancies (V_S) and Tin vacancies (V_{Sn}) [25]. This study reported that a Tin vacancy resulted in two localized levels, at -12.6 eV and $+0.31$ eV. The -12.6 eV defect energy level, within the valence band, corresponds to an energy level of electron in 's' orbital, while the $+0.31$ eV defect level lies within the forbidden gap. Jahangir et al. [25]. Showed that a Sulphur vacancy also creates a defect level within the forbidden gap at 0.37 eV. Vidal et al. [26] with DFT calculations have addressed the issue of Sn interstial defects too. However, these studies have not been directed to address most of the experimental observations, especially those related to samples with defects. Considering Tin Sulphide's commercial importance as a potential active layer in solar cells it becomes essential to address these gaps in our knowledge about SnS.

Tin Sulphide exists in many crystalline states. The orthorhombic structure ($a \gg b \approx c$) with *Pnma* 62 space group has received the maximum attention [24]. Ab-initio studies have been done on the influence of high pressure were performed for several orthorhombic IV-VI compounds in the *Pnma* symmetry GeS, GeSe, SnS and SnSe [27], while phase transitions were observed in SnS and SnSe crystals at high temperatures [28,29] and in a SnS crystal under pressure [30]. Ab-inito calculations by Gashimzade et al. [31] have shown the existence of the second order phase transition (*Pcmn* to *Cmcm*) near the pressure of 16 GPa. In this state, SnS unit cell contains eight atoms organised in two adjacent double layers caused by zig-zag bonds between Sn and S atoms. These layers are perpendicular to the direction of the unit cell's largest axis. SnS with orthorhombic unit cell ($c \gg a \approx b$) can also exist with C2mb 39 space group symmetry [32]. This structure too consists of double layers in parallel planes (similar to *Pmna*-62) however, with greater intra-plane packing (i.e. the thickness of the double layer is less

than that found in unit cells with *Pnma* symmetry) and Sn atoms barely protrude from the planes of Sulphur (see Fig. 1). In this study, we make theoretical calculations of the band structure of SnS and its optical properties and compare them with the results reported by Gupta et al. [15]. The study reported experimental results of SnS thin films whose X-Ray Diffraction data matched those given in ASTM Card 79-2193 (C2mb-39). However, residual tensile stress were found to exist in the reported samples. Also, it showed that the reflecting plane's orientation changed with increasing film thickness. The films orientation was found to move from 'ab' planes parallel to the substrate in thin films to an orientation where these planes became perpendicular to the substrate (thicknesses > 1000 nm). This meant that when light is incident perpendicular to the thinner films, it would be incident perpendicular to the 'ab' plane of the SnS unit crystal (i.e. perpendicular to plane [001] and along 'c' axis shown in Fig. 1 (b)). Similarly, incident light would probe the direction along to the 'ab' plane in thicker samples (i.e. perpendicular to plane [100] shown in Fig. 1(c)). Thus providing an interesting scope for investigating the anisotropic behavior of the SnS crystal. We have looked into the anisotropic optical properties of p-SnS here (dielectric function 'ε_2', refractive index 'n' and extinction coefficient 'k'). Further, these films were found to have p-type conductivity. This type of conductivity arises due to Tin vacancies. Defects such as vacancies also give rise to residual stresses within the film which in turn effects the material's band gap and optical behavior such as refractive index, extinction coefficient etc. Hence, experimentally, it is impossible to isolate the contribution of the two, i.e. of residual stress and vacancies. However, theoretically, we are at a liberty to investigate the contributions of each individually.

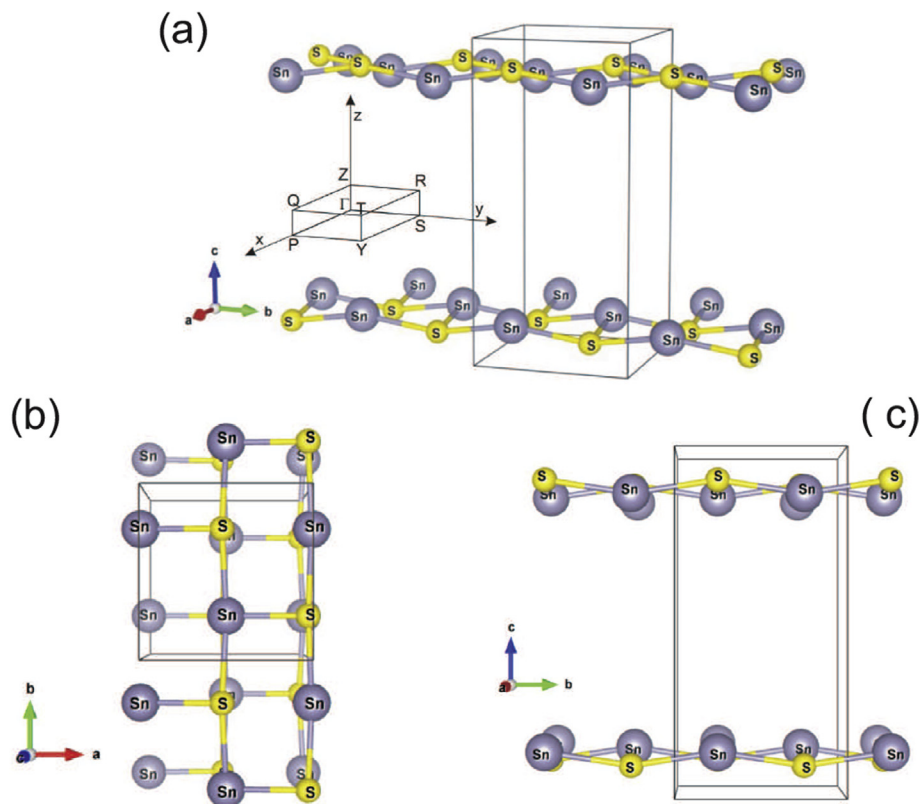It is in this direction that this study is based. In this manuscript,

Fig. 1. Different views of the C2mb 39 ortho-rhombic structure of SnS with (a) showing structure and Brillouin zone, while (b) and (c) shows the projection on the [001] and [100] planes, respectively.

we have made theoretical calculations of the band-gap, density of states (DOS), band structure and optical parameters (dielectric function, refractive index and extinction coefficients) for five situations. The first calculations were made for SnS with lattice parameters given in ASTM Card 79-2193, followed by calculations for lattice parameters of experimentally reported 450 nm and 870 nm thick SnS films [15] (henceforth referred as CI and CII, respectively). Nomenclature used for all the samples are listed in Table 1. The lattice parameters of the films were different from that given in the ASTM Card, indicating that residual stress existed in the films. The same calculations made for CI and CII were repeated by removing tin atoms, thus simulating vacancies in the crystal.

2. Theoretical methodology

All calculations in this study were done in the framework of the density functional theory (DFT) using generalized gradient approximation (GGA), within the parameterization of Perdew–Burke–Ernzerhof (PBE) [33], for the exchange and correlation potential as implemented in the ABINIT software package [34]. The eigenvalues and eigenfunctions of the Kohn–Sham [35] equations were solved self-consistently using the Projector Augmented Wave method (PAW) with atomic datasets available [36] for the expansion of the wave function, with a cutoff energy of 25 Ha, and a Monkhorst and Pack [37] grid to sample the Brillion zone (864 and 108 k-point for a unit cell and super cell systems, respectively). The cut-off energy of 25 Ha was found to be adequate for this and similar systems [27,38]. These parameters yielded a convergence of the total energy better than 10^{-5} Ha. As stated earlier, we carried out calculations of the electrical and optical properties for three SnS systems, namely pure/bulk, stressed, and stressed with Sn vacancies. In the case of the pure system, we performed the calculations of band structures, DOS, and optical properties using a unit cell (8 atoms) with lattice parameter of C2mb-39 symmetry given in ASTM Card 79-2193. We have also done calculations with/without spin-orbit coupling. For the stressed systems, we considered supercells of 64 atoms (8 unit cells) using the experimental lattice parameter, which were kept fixed during the process of self-consistent calculations. Vacancies in the crystal were simulated removing one Sn atom in these stressed supercells (i.e. 1.6% of vacancies). In the theoretical scheme, the vacancy implies considering a supper-lattice of 8 unit cells and removing one Sn atom from the lattice point common to all eight unit cells. In order to perform a detailed analysis of the optical transitions in SnS-stressed and SnS with stress and vacancy systems, we used a scissors approximation for correcting the differences between DFT calculations and experimental band gaps. Thus, theoretical band gaps were increased by 0.78 eV (in CI calculations) and by 0.70 eV (in CII calculations). All the calculations on supercell systems were performed without spin–orbit coupling.

3. Results and discussions

3.1. Electronic structure of bulk SnS

Fig. 2(a) and (b) shows the DOS and band structure, respectively of bulk SnS. The partial DOS indicate an important contribution of s-cation states to the top of the valence band (see in top of Fig. 2(a)) which hybridized with the p-cation and p-anion contributions define the main physical properties. Similar behavior was also found in *Pnma*-62 group symmetry [24]. In Fig. 2(b), we have displayed the calculated band structure in the directions Q→P→Γ→Z and Z→T→Y→S→R, with and without the inclusion of the spin-orbit coupling (SOC). The band-gap (E_g), with and without the spin-orbit coupling calculations does not introduce significant changes (the differences being less than 1% between the two methods of calculations). The band-gap using non-SOC calculations was 0.98 eV, while with the SOC interaction band-gap evaluated was 0.97 eV. Even more, the whole band structures in the different directions of the BZ remain the same, as can be seen in Fig. 2(b) and (c). Our calculations allow a comprehensive assessment of hybridization along the different directions of SnS. It is remarkable that in both calculations (SOC and non-SOC) the band structures coincide at the high symmetry points (Q, P, Γ, etc), with only a slight splitting in the conduction band. This however, does not relocate the band gap in the BZ. This behavior is significantly different from that reported for SnS in the *Pnma* (62) space group [24], where it was found that the spin-orbit coupling not only introduces splittings of energy levels in some regions of the band structure but also relocates the band gap in the BZ. This could be attributed to the fact that there are no heavy element atoms present in this structure. Also, the inter-layer separation between 'ab'-planes in SnS with C2mb symmetry is greater than that compared to the crystal with *Pnma* symmetry. This large inter-layer separation leads to a lower hybridization between the states of different planes. Due to this the band state hybridizations are strongly associated with the layered symmetry rather than with the spin-orbit interaction [27]. As mentioned, SnS-*Pnma* structure consists of double layers stacked onto each other along the a-axis, with each atom coordinated by three bound neighbors in the layer (bonds lengths being of the order of 2.6 to 2.7 Å) and one in the adjacent layer (inter-layer separation being 3.5 Å) [24,30], while in the SnS-C2mb structure the distance between an atom and its first neighbors is 2.72.9 Å and the inter-layer separation being 9.1 Å(this leads to the unit cell volume of C2mb is approximately double that corresponding to the *Pnma* symmetry). This large inter-layer separation leads to a lower hybridization of states between the different planes, reducing the spin-orbit interaction. With regards of the band gap energy, our calculations show that the maximum of the valence band (VBM) occurs at V1, V2 and V3 sites, defining a direct band-gap of 0.98 eV at Z (V2→C2), in competition with other two gaps, a direct gap between V1→C1 on Γ (1.06 eV), and an indirect gap between V3→C2, where V3 is located at about 3/4 from the Z point on the Z→T direction of the BZ (see Fig. 2b). In fact, in previous studies [27], it was demonstrated that SnS in the *Pnma* space group, and

Table 1
Lists the names given to various samples under study. For samples 2-5, the incident light is assumed to be incident perpendicular to 'ab' plane unless specifically mentioned (as in Figs. 6 and 7).

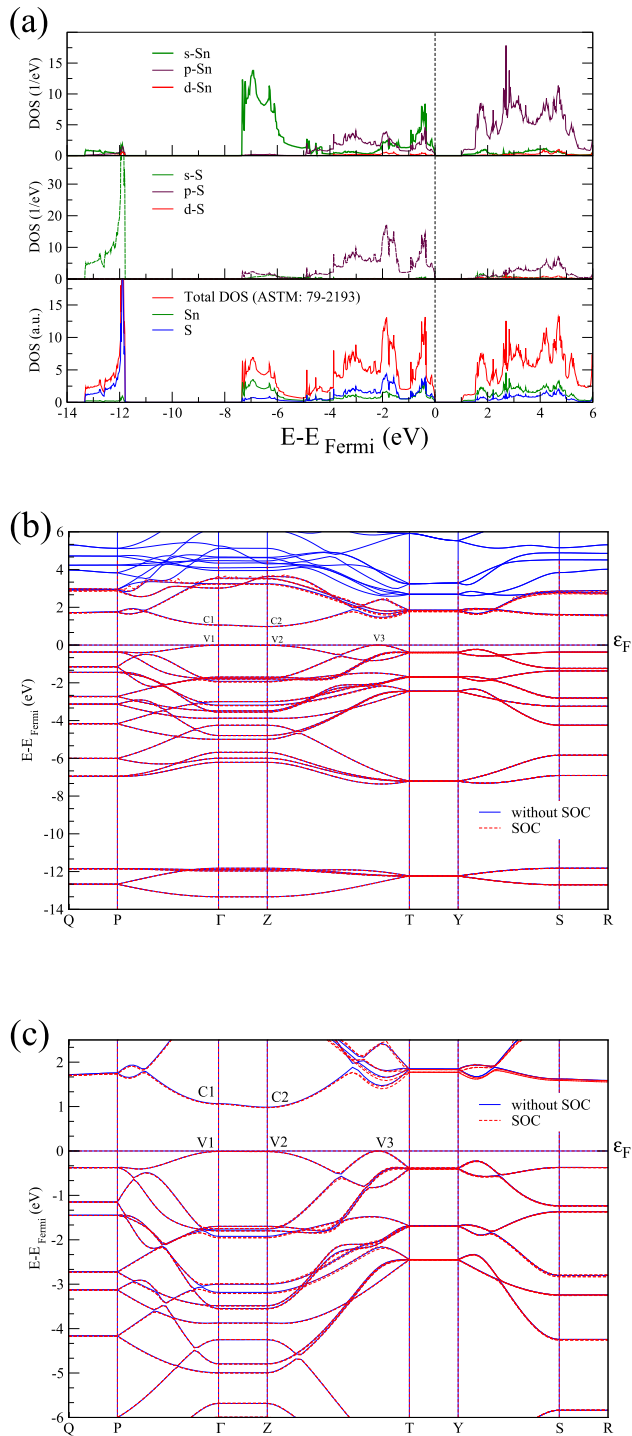| S.No.	Sample Description	Name
1.	Lattice parameter as in ASTM Card 79-2193 (5.673 Å, 5.750 Å, 11.760 Å)	Bulk
2.	5.690 Å, 5.773 Å, 11.778 Å of 450 nm film with residual stress	CI
3.	5.702 Å, 5.750 Å, 11.679 Å of 870 nm film with residual stress	CII
4.	CI with Sn vacancies	CI-V
5.	CII with Sn vacancies	CII-V

(a)

(b)

(c)

Fig. 2. (a) Shows the total DOS and local DOS of bulk SnS, (b) shows band structure of bulk SnS with and without spin-orbit coupling in different path in the Brillouin zone and (c) shows the same (Fig. 2b) on a reduced energy scale.

their related IV-VI orthorhombic compounds, exhibit several direct and indirect gaps which are close in energy and compete to form the band gap. However, there are almost no reports on the band structures in SnS with the C2mb symmetry [32], hence our present studies not only investigates the influence of the defects in SnS but also contributes to the knowledge of the bulk C2mb-SnS system in itself.

3.2. Electronic structure of SnS, stressed and vacancies with stress

3.2.1. Density of states

Fig. 3(a) shows the density of state calculated for the samples CI and CII. The states have been translated to fix the Fermi energy level at 0 eV. The DOS of the two cases seem very similar, however, zooming into the figure around the conduction band edge (Fig. 3 b) one can appreciate the difference.

Fig. 3(b) is a highly magnified plot of the DOS which compares the calculation results for CI and CII samples with that of CI-V and CII-V samples. As indicated by the arrows, the conduction level moves to higher energy levels with introduction of vacancies in the samples. In practical samples a 1.6% tin vacancy is not distributed uniformly throughout the crystal/grain. Hence, mixed phase exists in the crystal. This results in a smearing or spread of the energy levels (shown by shaded regions in Fig. 3(b)). This spread contributes to an exponential tailing in the absorption spectra. This is called the Urbach tail. From the DOS diagram of Fig. 3(b), we find the spread to be 0.02 eV and ≈0.015 eV for CI and CII samples, respectively. This suggests that the constant 1.6% vacancy simulated in our theoretical calculations results in the same amount of spread. In other words, the Urbach tail manifests due to defects such as vacancies and its magnitude reflects number/concentration of defects present. Similar suggestions of structural disorder giving rise to band tail or Urbach energy has been made in literature [39–41] and references therein. However, most of these studies have not tried to isolate the contribution of stress and defects. There are some scattered reports where amorphous solids [42–44] with defects have been studied in an attempt to avoid contributions arising from lattice parameters. Also, since the material in study were amorphous in nature, a semi-classical model was used to find the band-gaps from Joint Density of States [45]. As an end note, it is important to state here that experimentally the Urbach tail was found to increase from 0.084 to 0.235 eV for film thickness 450 (CI-V) and 870 nm (CII-V), respectively. Thus, indicating that the vacancy concentration was not constant as we had adopted in our theoretical calculations but increases with increasing film thickness.

Based on our results (see Table 2 and Fig. 4), we can conclude that in samples with vacancies (CI-V and CII-V), the Sn or cationic vacancies lead to appearance of energy levels into the forbidden gap near the valance band edge (see the shallow level SL in Table 2). This shallow acceptor state is created from the p-orbital of the anion hybridized with the s-orbital and the p-orbital of the cation states. As can be seen in Fig. 4(a) for sample CI-V, such hybridization occurs between the first and second nearest neighbors pairs of vacant site, i.e. S and Sn atoms, respectively. With reference to the cationic spectra, we can explain the C1 and C2 structures of Taniguchi et al. [46] as originated from a cooperative effect produced by relatively flat bands in different regions of the BZ, like that shown in Figs. 4 and 5 also for CI-V sample, together with the rest of the mixed bands about each energy in the whole BZ. As listed in Table 2 for stressed systems, our first peak in CI sample is at 1.91 eV, 0.08 eV above the conduction band minimum (CBM) (1.88 eV, 0.10 eV above the CBM, for CII), while our second peak is also well defined at 2.10 eV, 0.27 eV above CBM (2.06 eV, 0.18 eV above the CBM, for CII). Maintaining the same distortion of these systems (i.e, the same lattice parameter), the removal of cations causes a shift towards higher energies of the peaks C1 and C2 (see Fig. 4 and Table 2). The effect of the vacancy on the electronic properties is more noticeable in the system CI-V, which presents greater tensile stress along the 'ab' axis. The latter could be one of the causes for which the energies involved in the optical behavior of the CI-V system are greater than those associated with the CII-V system (see Table 3).
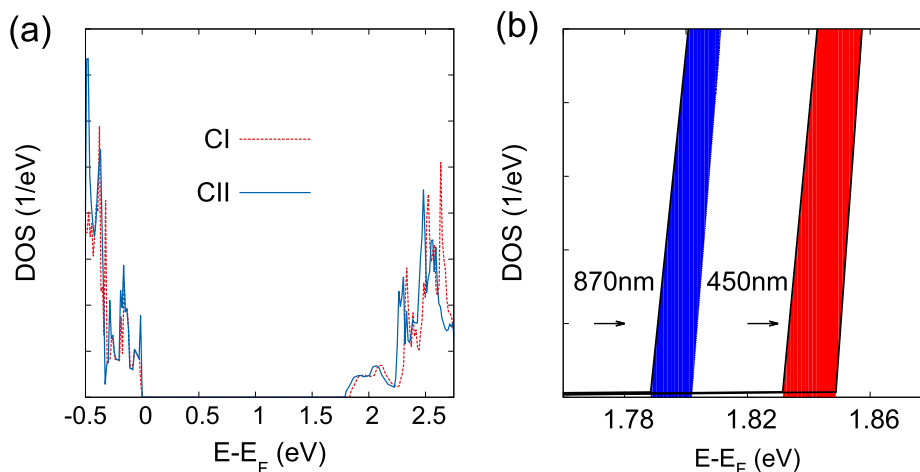
Fig. 3. (a) Compares the total DOS of CI and CII, (b) shows the spread in conduction band edge when Sn vacancies are introduced (as determined from total DOS calculations).
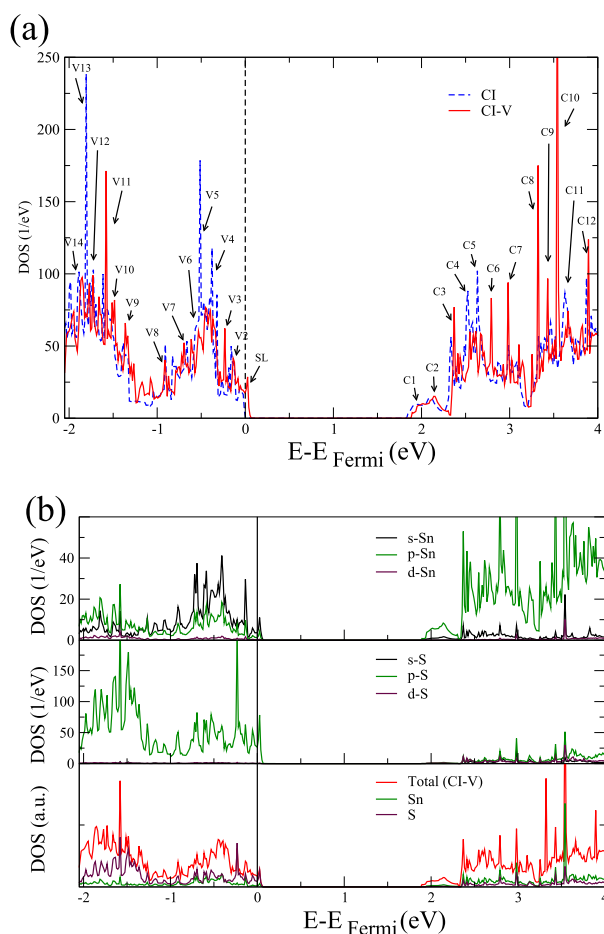

Fig. 4. Calculated density of states of the CI and CI-V, total-DOS (Left) and local-DOS (right). The first and second neighbors of the vacant site are indicated with S (49) and Sn (27) atoms, respectively. The Fermi energy ($E_F = 0$ eV), is at the bottom of the impurity band (vacancy states).

Table 2
Lists the main peaks of total-DOS of all samples (stressed and with vacancies). Also, to facilitate discussions, we present the composition of each peaks (atom and states) in decreasing order. We name SL as shallow level, V2 through V14 for the valence bands peaks and C1 through C12 for conduction band peaks of the DOS as they are shown in figure (Fig. 4).

Peak	DOS energy (eV)				Contributing States	
	CI	CI-V	CII	CII-V	main	minor
SL	–	0.06	–	0.04	p-S; s-Sn	p-Sn
V2	−0.15	−0.13	−0.17	−0.15	p-S; s-Sn	p-Sn
V3	−0.27	−0.23	−0.28	−0.25	p-S	s-Sn, p-Sn
V4	−0.38	−0.40	−0.38	−0.38	p-S; s-Sn	p-Sn, d-Sn
V5	−0.51	−0.45	−0.48	−0.46	p-S	p-Sn, d-Sn
V6	–	−0.61	–	−0.62	p-S; s-Sn	p-Sn, d-Sn
V7	−0.67	−0.69	−0.67	−0.71	p-S; s-Sn	p-Sn, d-Sn
V8	−0.90	−0.92	−0.97	−0.93	p-S; s-Sn	p-Sn, d-Sn
V9	−1.39	−1.36	−1.37	−1.36	p-S	s-Sn, p-Sn
V10	−1.53	−1.50	−1.57	−1.53	p-S	s-Sn, p-Sn
V11	−1.61	−1.58	−1.61	−1.60	p-S; s-Sn, p-Sn	d-Sn
V12	−1.73	−1.73	−1.72	−1.72	p-S	s-Sn, p-Sn
V13	−1.81	−1.78	−1.78	−1.78	p-S; s-Sn, p-Sn	d-Sn
V14	−1.89	−1.85	−1.92	−1.91	p-S; s-Sn, p-Sn	d-Sn
C1	1.91	1.98	1.88	1.91	p-Sn	s-Sn; p-S, d-S
C2	2.10	2.15	2.06	2.10	p-Sn	s-Sn; p-S, d-S
C3	2.33	2.37	2.28	2.28	p-Sn	s-Sn; s-S, p-S, d-S
C4	2.52	2.55	2.47	2.47	p-Sn	s-Sn; s-S, p-S, d-S
C5	2.64	2.68	2.58	2.60	p-Sn	s-Sn; s-S, p-S, d-S
C6	–	2.80	2.74	2.74	p-Sn	s-Sn; s-S, p-S, d-S
C7	2.98	3.00	2.93	2.93	p-Sn	s-Sn; s-S, p-S, d-S
C8	3.34	3.33	3.27	3.27	p-Sn	s-Sn; s-S, p-S, d-S
C9	3.45	3.43	3.34	3.35	p-Sn	s-Sn; s-S, p-S, d-S
C10	3.52	3.54	3.43	3.47	p-Sn	s-Sn; s-S, p-S, d-S
C11	3.63	3.66	3.55	3.54	p-Sn	s-Sn; s-S, p-S, d-S
C12	3.88	3.90	3.80	3.80	p-Sn	s-Sn; s-S, p-S, d-S

3.2.2. Energy bands

SnS has an orthorhombic layered structure as shown in Fig. 1(a). While covalent to ionic bonds are present between Sn and S atoms in the 'ab' plane, Van der Waal's forces are present between adjacent layers along the 'c'-axis. In Fig. 5 we plot the calculated band structure in the directions P→Γ→Z→T→Y of the CI and CI-V supercells, as representative of the systems with stress and stress with defects, respectively. All calculations on supercell systems for this figure were performed without spin-orbit interaction, since SOC has a negligible effect (as discussed in sections above). As can be seen in Fig. 5, the competition between transitions to form the band-gap is also observed both in stressed systems and systems with vacancies, but contrary to what was found in the system without defects (Fig. 2(b)), in all the samples with defect, the band-gap occurs in the Γ − point (0.04 eV lower than at Z-point). It is observed that the VBM associated to V3 in the pure system (see Fig. 2(b)), shows a displacement towards the Z point in the system with defects, now being located at about 1/2 from the Z point of the
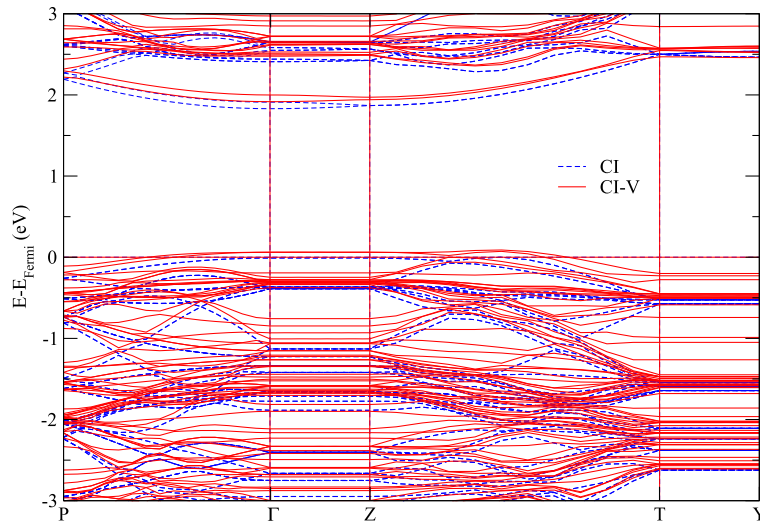
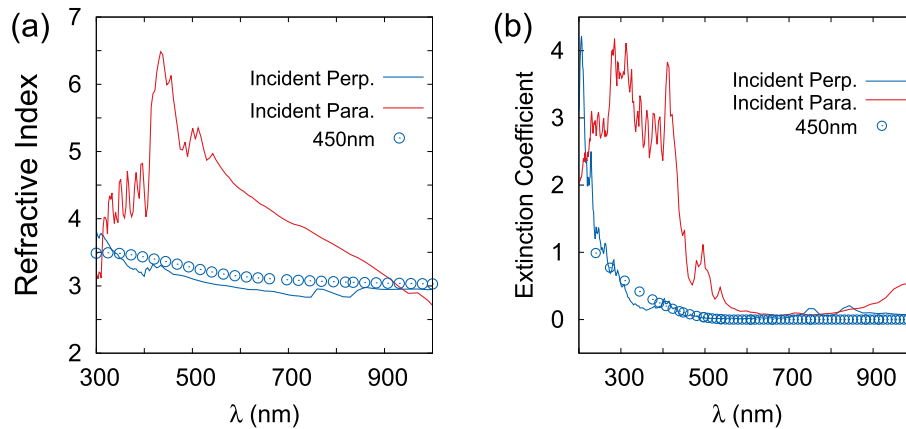**Fig. 5.** The band structure of CI (stressed) and CI-V (CI with vacancy).

Fig. 6. The (a) refractive index (n) and (b) the extinction coefficient (k) of CI stressed sample (450 nm films) determined using the SE ellipsometry data (shown by circles) compared to that evaluated theoretically, as a function of light wavelength.

$Z{\to}T$ direction of the BZ (see Fig. 5). We notice that the directions involving 'ab'-plane (i.e. directions $P{\to}\Gamma$, $Z{\to}T$, or $Z{\to}Q$ in Fig. 6(b)) are the most hybridized, where spreading and crossing of bands is increased. The bands over the $\Gamma{\to}Z$ and $T{\to}Y$ line, corresponding to the largest lattice parameter 'c' (see Fig. 1(a)), i.e. along the axis perpendicular to the cleavage plane of the crystal, however, are less symmetrical with fewer hybridization. Also, as can be seen in Fig. 5, even though systems with vacancies have band structure characteristics similar to that of the stressed system (for example the band gap is maintained in Γ point and maintains or has similar crossing of bands, etc.), the main difference is the spreading of bands vs. energy in samples with vacancies, mainly in bands in the directions $\Gamma{\to}Z$ and $T{\to}Y$ (along the axis with Van der Waal's forces).

In the following section we shall investigate the contribution of stress and vacancy on the optical properties of SnS thin film.

3.3. Optical properties of SnS samples with stress and vacancies

We have determined the imaginary part of the complex dielectric function $\varepsilon_2(\omega)$, using the standard tetrahedron-method corrected by the "scissor" operator as mentioned above. The real part of the diagonal dielectric functions was computed from $\varepsilon_2(\omega)$ using the Kramers-Kroning relations [47]. In order to achieve a

comprehensive understanding of the optical behavior of the system, along with the complex dielectric function, the refractive index, $n(\omega)$, extinction coefficient and $k(\omega)$ were calculated for polarized light incident along the three main axes of the crystal. All the four systems presented a triaxial anisotropy (different properties along the 'a', 'b' and 'c' axis) for different ranges of incident photon energy. However, since the perturbations in ab-plane direction (see 'ab' directions in Fig. 1(b)), are almost the same in all ranges of energy (a consequence of $a{\approx}b$), we have taken the average value of the calculated optical property along 'a' and 'b' axis and have indicated the average when light is 'incident perpendicular' to the 'ab' plane in Fig. 6(a).

Fig. 6 (a) and (b) compares the refractive index and the extinction coefficient of CI-V determined experimentally using the Spectroscopic ellipsometry data [48] as a function of incident light's wavelength to that evaluated theoretically. The theoretical calculations were made for light incident perpendicular and parallel to 'ab' crystal plane. The strong anisotropic behavior of SnS along these two directions is clearly evident. As can be seen from Fig. 6(a) and (b) the experimental data for both refractive index and extinction coefficient are in good agreement with the values obtained theoretically for the case of light incident perpendicular to the 'ab' plane. We hence conclude that our theoretical calculations
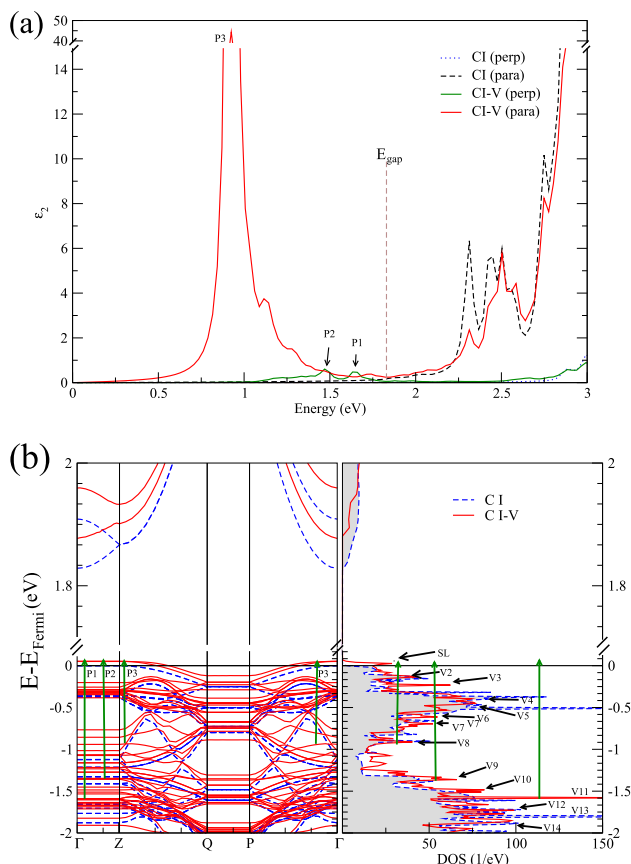
Fig. 7. Calculated (a) dielectric function (imaginary parts) for CI and CI-V, (b) Band structure and total DOS which includes the transitions associated with the peaks of interest.

Table 3
Optical transitions of perturbations perpendicular to the 'ab' plane, from ε_2 and DOS calculations.

Peak	DOS		ε_2	
	CI-V	CII-V	CI-V	CII-V
P1 (V11-SL)	1.64	1.64	1.65	1.58
P2 (V9-SL)	1.41	1.40	1.47	1.40
P3 (V8-SL)	0.98	0.97	0.93	0.85

confirm the experimental results of 'ab' plane being parallel to the substrate as was reported by Gupta et al. [15]. Considering the above conclusion, all the results discussed hereafter are for orientation where light is incident perpendicular to the 'ab' plane only.

The imaginary part of the dielectric function shows typical response of a semiconductor with some fine structure (see Fig. 7(a)). The systems with vacancies shows greater anisotropy as compared to those with just stress. For both directions of perturbation, as a consequence of the cationic vacancy the absorption edge shows a red shift. Also, for energies higher than 3 eV, the optical properties show almost no change due to vacancies defect. A similar behavior was observed in deformed SnS when subjected to pressure [27]. A very sharp peak (P3) around 0.9 eV (perturbation parallel to 'ab' plane) is seen with two peaks (P2 and P1) around 1.4 and 1.6 eV (perturbation perpendicular to 'ab' plane). We have identified these peaks arising due to transitions from the shallow level (SL) appearing due to Sn-vacancy to V11, V9, and V8 peaks levels associated with p-S and s-Sn orbitals (see Table 1). The

energy values (Table 3) corresponding to transitions for all systems were evaluated from the DOS and band structure diagram (Fig. 7(b)). Since the present study is focussed on the photo-voltaic application of SnS, we have restricted our analysis to the visible region of the spectrum ($300 \leq \lambda \leq 1000$ nm) or up to an energy range of 3 eV. It is important to note that the appearance of the shallow level above the valence level and upward shift in conduction level (as seen by change is DOS level, Fig. 3(b)), both contribute to the Urbach tail and change the samples band-gap. It is given as

$$E_{g(new)} = E_g + (new\ CB) - (new\ VB)$$

Since the spread and shift in the conduction band level (CB) is not significant (≈ 0.02 eV), the equation clearly suggests a red-shift in band-gap with increasing thickness of p-SnS films due to increasing Sn defects. The result of this study clearly suggests that an increase in Sn vacancies results in a decrease in band-gap (red shift). A red-shift of band-gap with film thickness was also observed experimentally by Gupta et al. [15] and was explained due to size effect. Hence, the red shift reported experimentally maybe a commulative effect of increasing grain size and Sn vacancies (see Fig. 8).

In Fig. 9(a) and (b), we compare the theoretically evaluated refractive index and extinction coefficient of CI and CII stressed samples (those having no vacancies). There seem to be an insignificant variation in the two cases. Considering that the tensile stress induces a mere 0.01–0.02 Å elongation in the 'a/b' lattice parameter, this lack of variation in the theoretically simulated refractive index is hence not surprising. The variation of refractive index with incident light's wavelength seen in Fig. 9(a) for $\lambda > 450$ nm is typical of Cauchy's dispersion relation. Cauchy dispersion relation is valid only in the transparent region of the material, the zero (approx) value of extinction coefficient in the said wavelength region confirms the transparent nature of SnS unit cell experiencing only stress. However, Gupta et al. [15] using their experimental ellipsometry data have shown that the variation of SnS refractive index follows the Tauc Lorentz (TL) dispersion relation. This variation in dispersive relation is due to the vacancies present in the film. Fig. 9(c) and (d) compares the theoretical evaluation of the refractive index and extinction coefficients of CI-V
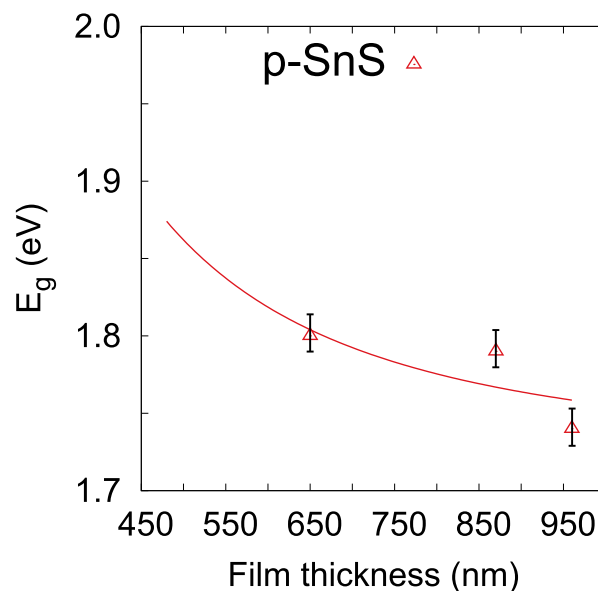

Fig. 8. Graph shows the experimentally observed variation in band gap with film thickness.
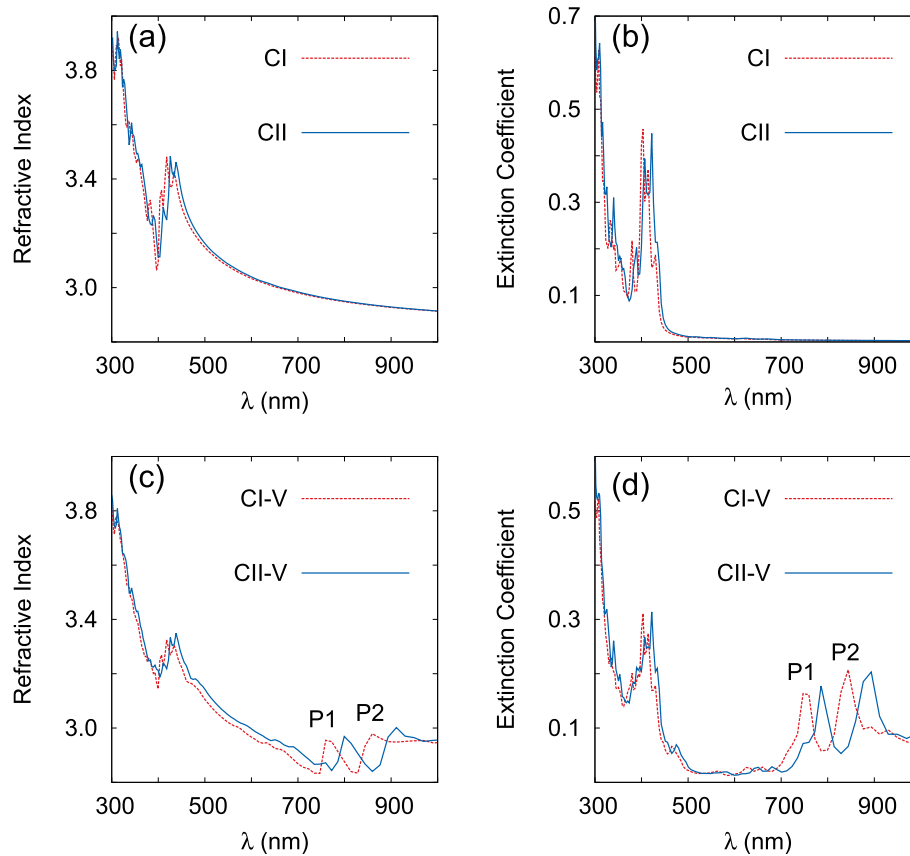
Fig. 9. The refractive index (n) and the extinction coefficient (k) of CI and CII samples (a and b) along with that of CI-V and CII-V (c and d).

and CII-V samples, respectively (having 1.6% tin vacancies). Notice that the difference in refractive index between the two samples is more pronounced now, especially for $\lambda \geq 500$ nm. Also, the transparent region is curtailed (extending only between $500 \leq \lambda \leq 700$ nm) due to appearance of appreciable absorption peaks for $\lambda \geq 700$ nm. Considering that the number of Sn vacancies in CI-V and CII-V were maintained same for calculations, the transition peak positions (P1 and P2) that appear due to defects, were found to be sensitive to the residual stress present. A red shift in P1 and P2 is evident due to the lattice deformation of 'a' and 'b' (see Fig. 9(c) and d). P1 and P2 peaks were absent in Gupta et al. experimental data (Fig. 6). This might be due to the low Sn vacancies present in the sample and the UV−visible spectrometer insensitive to the variations.

We hence believe that the residual stress effects the band-gap and optical properties of SnS thin films, however, the optical properties of SnS are more strongly influenced by the number of defects/vacancies. To further investigate this idea, we analyse the theoretical refractive index data using the Wemple-Dedomomenico (WDD) model. Although a large number of dispersion relations are available for the transparent region like Cauchy's, Sellmeier etc., WDD was selected as it gives an insight into the structural properties via its two fitting parameters (E_o and E_d) as will be seen in the following paragraphs.

3.3.1. Wemple-Dedomenico model

The Wemple-Dedomenico (WDD) model [49] quantifies the dispersive behavior of the material assuming that all the valance electrons of the material behave as oscillators with only single dominant oscillator. The WDD single oscillator model can be used to study the variation of refractive index with wavelength in the

transparent region ($550 \leq \lambda \leq 700$ nm), i.e. the region where the incident light's energy (E) is less than the material's band-gap ($E < E_g$). The WDD dispersion relation is given as [49]

$$n^2 = 1 + \frac{E_d E_o}{E_o^2 - E^2} \tag{1}$$

where E_o is the oscillator energy and E_d is the dispersion energy. While E_o quantifies the material's band-gap (it is proportional to E_g), E_d is related to the charge distribution in the unit cell and hence depends on the material's structure. E_d is given as

$$E_d = \beta N_c Z_a N e \tag{2}$$

where 'N_e', 'Z_a' and 'N_c' are the effective number of valence electrons per anion, the anion valency and the coordination number or the number of nearest neighboring cations, respectively. 'β' is a constant which is equal to 0.26 eV for ionic bonding and 0.37 eV for covalent bondings. Fig. 10(a) and (b) shows the WDD model fitting made on the theoretically obtained refractive index data for the stressed and stressed with vacancy samples, respectively. The two plots are in different wavelength regions depending on the transparent region or k≈0 region obtained. The values of E_o and E_d evaluated from the theoretical data for CI, CI-V, CII and CII-V along with those obtained from experimental SE data in the wavelength range $550 \leq \lambda \leq 700$ nm are listed in Table 4. Notice that the E_d values for sample CI-V sample is comparable not only with the experimental value but also with the E_d (theoretical) value of CII-V sample. This, we believe is due to the fact that theoretical computation of the refractive index for both, CI-V and CII-V samples, were made by assuming 1.6% Sn vacancy in SnS unit cell. Similarly, CI and
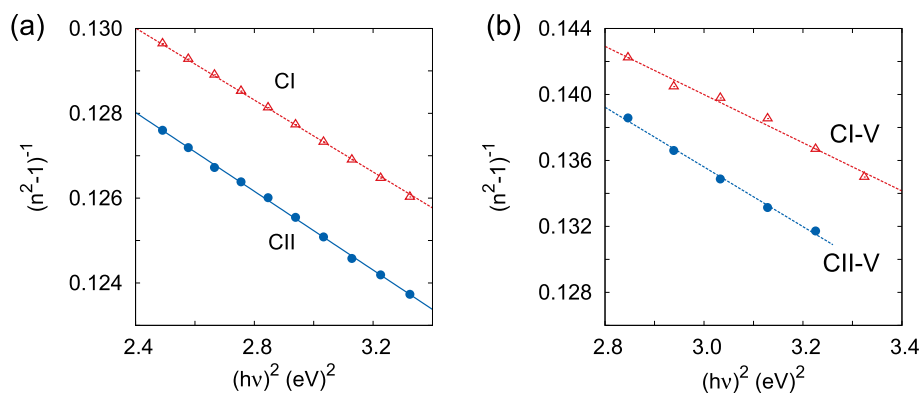
Fig. 10. (a) and (b) shows the WDD model fitting made on samples CI, CII and CI-V, CII-V, respectively.

Table 4
Coefficients of Wemple-Dedomenico model obtained from Theoretical estimation of refractive index and that from experimental Spectroscopic Elliptical (SE) data.

Sample	WDD Constants from Theory		WDD Constants from SE data	
	E_d (eV)	E_o (eV)	E_d (eV)	E_o (eV)
CI	41.00	7.750	–	–
CII	39.34	5.475	–	–
CI-V	24.60	3.510	22.65	3.344
CII-V	17.05	3.240	11.61	2.725

CII samples, also returned comparable values of E_d, with magnitudes higher than those obtained for samples with vacancies. In their work, Gupta et al. [15] had concluded that N_e and Z_a of Eq (2) are constant for SnS and any variation in E_d values is due to changes in βN_c. The variation in βN_c product is due to change in charge distribution in the unit cell due to defects present in the films. Clearly, from Table 4, it is clear that a decrease in E_d is indicative of an increase in defect/vacancy concentration. Hassanien et al. [50] have worked on the same lines but did not comment upon their listed data of dispersion energy, Urbach tail and Se concentration in $Cd_{50}S_{50-x}Se_x$ thin films. For first principle calculations, we have assumed a linear (with negative slope) relationship between E_d and vacancy concentration, the experimental sample of CII-V is projected to have 2.11% Sn vacancy. Based on the relationship between Urbach tail and E_d reported by Gupta et al. [48], it would further imply that the magnitude of band spread or Urbach tailing is a direct measure of vacancies present in the sample.

Thus, our calculations allow us to reproduce and predict the experimental results having only considered systems with an isolated vacancy, thus providing only that percentage of defects similar to the experimental one. This suggests that the effects associated with possible interactions between vacancies, would play a minor role compared to the effects of the imperfection itself within the lattice, although subsequent work could be needed to confirm it.

4. Conclusion

Theoretical calculations of the band-gap, density of states, band structure and optical properties were made for tin sulphide with C2mb-39 symmetry in bulk state and film state with residual stress and defects. It was found that even on including spin-orbit coupling in our calculations, it does not change the position of band-gap (at Γ – point and induce only slight splitting in conduction band. This observation is contrary to what is observed in SnS with *Pnma* space

group symmetry, where the spin-orbit interaction relocates the band gap in the Brillion Zone. Since spin-orbit coupling shows no major manifestation for SnS with C2mb-39 symmetry, all the calculations reported here were done without the spin-orbital interactions. These calculations were done to confirm and verify the experimental results in literature on p-SnS films. The tin vacancies responsible for p-type conductivity of SnS thin films also result in stress in the crystal lattice which in turn leads to spreading of band edges (or Urbach tail) within the forbidden band-gap. The Urbach tail was found to be increasing with film thickness. Band-gap of the as-grown films as calculated from absorption spectra using the Tauc's method was found to be the function of grain-size, lattice parameter and defects present in the films. Increasing grain-size and band edge spreading causes red-shift in the band-gap values. Thus, in terms of photon absorption for solar cell applications, increased band-spreading and grain size with thickness helps in lowering of band-gap and bringing it closer to optimum value required for solar cell application of 1.5 eV. Experimentally, the effects of stress and that of defects can not be isolated. However, theoretically we were at liberty to test the same. Calculations were made for samples with stress (CI, CII) and those stressed with vacancies (CI-V, CII-V). A spread in conduction band edge was observed for CI and CII samples after introduction of defect in the lattice, indicating the band spreading is a direct measure of the number of defects present in the lattice. To study the effect of defects, calculations were done by simulating absence of one Tin atom from a SnS unit cell (corresponding to 1.6% vacancies). Band-gap was found to decrease with inclusion of defects in the sample. Inclusion of Tin vacancy in crystal lattice creates a shallow defect level near the valance band edge in both the samples. The appearance of shallow defect level in both the samples (CI-V, CII-V) suggests a direct proportionality between the Urbach tail and defect concentration.

The theoretical calculations confirm the anisotropic properties of tin sulphides. It also confirms that the experimental results reported in discussed literature were of samples with the 'ab' crystal plane parallel to the substrate. Another interesting observation in theoretical results was the appearance of two absorption peaks at wavelength of 700 nm and 900 nm corresponding to the transition from valance band to shallow level only in when light is incident perpendicular to the 'ab' plane. A red shift was observed in CII-V samples as compared to CI-V sample, indicating that these peaks which arise due to defects are also sensitive to the stress present in the sample. Theoretically obtained refractive index matched to that obtained experimentally using spectroscopic ellipsometry. Fits of WDD model in transparent region of theoretical refractive index match those done with the experimental data. The decrease in

dispersion energy (E_d) shows an increased amount of vacancies for thicker samples (CII-V). From first principle calculations, assuming a linear relation between E_d and Tin vacancy concentration, the experimental 870 nm thick sample is predicted to have 2.11% vacancies.

Thus, the calculations of various properties of SnS are in total agreement with the experimental results.

Acknowledgement

References

[1] P. Sinsermsuksakul, J. Heo, W. Noh, A.S. Hock, R.G. Gordon, Atomic layer deposition of tin monosulfide thin films, Adv. Energy Mater. 1 (2011) 1116.

[2] H. Noguchi, A. Setiyadi, H. Tanamora, T. Nagatomo, O. Omoto, Characterization of vacuum-evaporated tin sulfide film for solar cell materials, Sol. Energy Mater. Sol. C 35 (1994) 325.

[3] J.A. Andrade-Arvizu, M. Courel-Piedrahita, O. Vigil-Galan, SnS-based thin film solar cells: perspectives over the last 25Years, J. Mater. Sci. Mater. Electron. 26 (2015) 4541.

[4] G.H. Yue, D.L. Peng, P.X. Yan, L.S. Wang, W. Wang, X.H. Luo, Structure and optical properties of SnS thin film prepared by pulse electrodeposition, J. Alloys Compd. 468 (2009) 254.

[5] C. Gao, H. Shen, L. Sun, Preparation and properties of zinc blende and ortho-rhombic SnS films by chemical bath deposition, Appl. Surf. Sci. 257 (2011) 6750.

[6] S.S. Hegde, A.G. Kunjomana, M. Prashantha, C. Kumar, K. Ramesh, Photovoltaic structures using thermally evaporated SnS and CdS thin films, Thin Solid Films 545 (2013) 543.

[7] M.M. El-Nahass, H.M. Zeyada, M.S. Aziz, N.A. El-Ghamaz, Optical properties of thermally evaporated SnS thin films, Opt. Mater. 20 (2002) 159.

[8] X. Jiaxiong, Y. Yang, Z. Xie, Fabrications of SnS thin films and Sns-based het-erojunctions on flexible polyimide substrates, J. Mater. Sci. Mater. Electron. 25 (2014) 3028.

[9] B. Ghosh, M. Das, P. Banerjee, S. Das, Fabrication of vacuum-evaporated SnS/CdS heterojunction for PV applications, Energy Mater. Sol. C 92 (2008) 1099.

[10] L.S. Price, I.P. Parkin, T.G. Hillbert, K.C. Molloy, Atmospheric pressure CVD of SnS and SnS2on glass, Chem. Vap. Depos. 4 (1998) 222.

[11] A.S. Juarez, A. Ortiz, Effects of precursor concentration on the optical and electrical properties of Sn_xS_yThin films prepared by plasma-enhanced chemical vapour deposition, Semicond. Sci. Technol. 17 (2002) 931.

[12] Z. Zainal, M.Z. Hussein, A. Ghazali, Cathodic electrodeposition of SnS thin films from aqueous solution, Sol. Energy Mater. Sol. C 40 (1996) 347.

[13] M. Calixto-Rodriguez, H. Martinez, A. Sanchez-Juarez, J. CamposAlvarez, A. Tiburcio-Silver, M.E. Calixto, Structural, optical, and electrical properties of tin sulfide thin films grown by spray pyrolysis, Thin Solid Films 517 (2009) 2497.

[14] K.S. Kumar, C. Manoharan, S. Dhanapandian, A.G. Manohari, Effect of Sb dopant on the structural, optical and electrical properties of SnS thin films by spray pyrolysis technique, Spectrochim. Acta Part A Mol. Biomol. Spectrosc 115 (2013) 840.

[15] Y. Gupta, P. Arun, Suitability of SnS thin films for photovoltaic application due to the existence of persistent photocurrent, Phys. Status Solidi 253 (2016) 509.

[16] W. Albers, C. Haas, H.J. Vink, J.D. Wassche, Investigations on SnS, J. Appl. Phys. 2 (1961) 2220.

[17] Y. Gupta, P. Arun, A.A. Naudi, M.V. Walz, E.A. Albanesi, Grain size and lattice Parameter's influence on band gap of SnS thin nano-crystalline films, Thin Solid Films 612 (2016) 310.

[18] P. Jain, P. Arun, Influence of grain size on the band-gap of annealed SnS thin films, Thin Solid Films 548 (2013) 241.

[19] Y. Gupta, P. Arun, Optimization of SnS active layer thickness for solar cell application, J. Semicond. 38 (2017) 113001.

[20] S. Sohila, M. Rajalakshmi, C. Ghosh, A.K. Arora, C. Muthamizhchelvan, Optical and Raman scattering studies on SnS nanoparticles, J. Alloys Compd. 509 (2011) 5843.

[21] R.E. Banai, M.W. Horn, J.R.S. Brownson, A review of tin (II) monosulfide and its potential as a photovoltaic absorber, Sol. Energy Mater. Sol. C 150 (2016) 112.

[22] Y. Kumagai, L.A. Burton, A. Walsh, F. Oba, Electronic structure and defect physics of tin sulfides: SnS, Sn_2S_3, and SnS_2, Phys. Rev. Appl. 6 (2016) 014009.

[23] T.J. Whittles, L.A. Burton, J.M. Skelton, A. Walsh, T.D. Veal, V.R. Dhanak, Band alignments, valence bands, and core levels in the tin sulfides SnS, SnS_2, and Sn_2S_3: experiment and theory, Chem. Mater. 28 (2016) 3718.

[24] L. Makinistian, E.A. Albanesi, On the band gap location and core spectra of orthorhombic IV-VI compounds SnS and SnSe, Phys. Status Solidi B 246 (2009) 183.

[25] Z.A. Jahangirli, Self-consistent calculations of the electronic structures of deep Sn and S vacancy levels in SnS by the method of Green functions, Russ. J. Chem. A 84 (2010) 1536.

[26] J. Vidal, S. Lany, M. d'Avezac, A. Zunger, A. Zakutayev, Band-structure, optical properties, and defect physics of the photovoltaic semiconductor SnS, Appl. Phys. Lett. 100 (2012) 032104.

[27] L. Makinistian, E.A. Albanesi, Study of the hydrostatic pressure on ortho-rhombic IV-VI compounds including many-body effects, Comput. Mater. Sci. 50 (2011) 28722879.

[28] H. Wiedemeier, F.J. Csillag, The thermal expansion and high temperature transformation of tin monosulfide and tin selenide, Z. Kristallogr. 149 (1979) 17.

[29] H.G.V. Schnering, H. Wiedemeier, The high temperature structure of $\beta-$SnS and $\beta-$SnSe and the B16-to-B33 type λ-transition path, Z. Kristallogr. 156 (1981) 143.

[30] L. Ehm, K. Knorr, P. Dera, A. Krimmel, P. Bouvier, M. Mezouar, Pressure-induced structural phase transition in the IVVI semiconductor SnS, J. Phys. Condens. Mater. 16 (2004) 3545.

[31] F.M. Gashimzade, D.A. Guseinova, Z.A. Jahangirli, B.G. Mekhtiev, Second-order phase transition in a SnS orthorhombic crystal under pressure, Phys. Solid State 57 (2015) 378.

[32] G.A. Wiegers, Misfit layer compounds: structures and physical properties, Prog. Solid State Chem. 24 (1996) 1.

[33] J.P. Perdew, K. Burke, M. Ernzerhof, Generalized gradient approximation made simple, Phys. Rev. Lett. 77 (1996) 3865.

[34] X. Gonze, B. Amadon, P.M. Anglade, J.M. Beuken, F. Bottin, P. Boulanger, F. Bruneval, D. Caliste, R. Caracas, M. Cote, T. Deutsch, L. Genovese, Ph Ghosez, M. Giantomassi, S. Goedecker, D. Hamann, F. Jollet, G. Jomard, S. Leroux, M. Mancini, S. Mazevet, M.J.T. Oliveira, G. Onida, Y. Pouillon, T. Rangel, G.M. Rignanese, D. Sangalli, R. Shaltaf, M. Torrent, M.J. Verstraete, G. Zrah, J.W. Zwanziger, Comput. Phys. Commun. 180 (2009) 2582.

[35] W. Kohn, L.J. Sham, Self consistent equations including exchange and corre-lation effects, Phys. Rev. 140 (1965) 1133.

[36] F. Jollet, M. Torrent, N. Holzwarth, Generation of Projector Augmented-Wave atomic data: a 71 elements validated table in the XML format, Comput. Phys. Commun. 185 (2014) 1246.

[37] H.J. Monkhorst, J.D. Pack, Special points for brillouin-zone integrations, Phys. Rev. B 13 (1976) 5188.

[38] L.C. Gomes, A. Carvalho, Phosphorene analogues: isoelectronic two-dimensional group-IV monochalcogenides with orthorhombic structure, Phys. Rev. B 92 (2015) 085406.

[39] D. Nesheva, Z. Levi, Z. Aneva, V. Nikolova, H. Hofmeister, Experimental studies on the defect states at the interface between nano-crystalline cdse and amorphous SiO_x, J. Phys. Condens. Matter 12 (2000) 751.

[40] N. Nicoloso, A. Lobert, B. Leibold, Optical absorption studies of tetragonal and cubic thin film yttria-stabilized zirconia, Sens. Actuators, B 8 (1992) 253.

[41] J.I. Pankove, Absorption edge of impure gallium arsenide, Phys. Rev. 140 (1965) A2059.

[42] G.D. Cody, T. Tiedje, B. Adeles, B. Brooks, Y. Goldstein, Disorder and optical absorption edge of hydrogenated amorphous silicon, Phys. Rev. Lett. 47 (1981) 1480.

[43] J.H. Dias da Silva, R.R. Campomanes, D.M.G. Leite, Relationship between the optical gap and the optical-absorption tail breadth in amorphous gaas, J. Appl. Phys. 96 (2004) 7052.

[44] A. Skumnich, A. Frova, N.M. Amer, Urbach tail and gap states in hydrogenated a-Sic and a-Sige alloys, Solid State Commun. 54 (1985) 597.

[45] S.K. O'Leary, Optical absorption, disorder and the disorderless limit in amor-phous semiconductors, Appl. Phys. Lett. 72 (1998) 1332.

[46] M. Taniguchi, R.L. Johnson, J. Ghijsen, M. Cardona, Core excitons and conduction-band structures in orthorhombic GeS, GeSe, SnS, and SnSe single crystals, Phys. Rev. 42 (1990) 3634.

[47] P.Y. Yu, M. Cardona, Fundamentals of Semiconductors Physics and Materials Properties, Springer, Boston, MA, United States, 2010.

[48] Y. Gupta, P. Arun, Influence of Urbach tail on the refractive index of p-SnS thin films, Phys. Status Solidi C 14 (2017) 1600207.

[49] S.H. Wemple, M. DiDomenico, Behavior of the electronic dielectric constant in covalent and ionic molecules, Phys. Rev. B 3 (1971) 1338.

[50] H.S. Hassanien, A.A. Akl, Influence if composition on optical and dispersion parameters of thermally evaporated non-crystalline $Cd_{50}S_{50-x}Se_x$ thin films, J. Alloys Compd. 648 (2015) 280.